MLS and CALIOP Cloud Ice Measurements in the Upper Troposphere: A Constraint from Microwave on Cloud Microphysics

DONG L. WU

NASA Goddard Space Flight Center, Greenbelt, Maryland

ALYN LAMBERT AND WILLIAM G. READ

Jet Propulsion Laboratory, California Institute of Technology, Pasadena, California

PATRICK ERIKSSON

Department of Earth and Space Science, Chalmers University of Technology, Göteborg, Sweden

JIE GONG

Universities Space Research Association, NASA Goddard Space Flight Center, Greenbelt, Maryland

(Manuscript received 14 January 2013, in final form 14 August 2013)

ABSTRACT

This study examines the consistency and microphysics assumptions among satellite ice water content (IWC) retrievals in the upper troposphere with collocated A-Train radiances from Microwave Limb Sounder (MLS) and lidar backscatters from Cloud–Aerosol Lidar with Orthogonal Polarization (CALIOP). For the cases in which IWC values are small ($<10\,\mathrm{mg\,m^{-3}}$), the cloud ice retrievals are constrained by both MLS 240- and 640-GHz radiances and CALIOP 532-nm backscatter β_{532}. From the observed relationships between MLS cloud-induced radiance T_{cir} and the CALIOP backscatter integrated γ_{532} along the MLS line of sight, an empirical linear relation between cloud ice and the lidar backscatter is found: IWC/β_{532} = 0.58 ± 0.11. This lidar cloud ice relation is required to satisfy the cloud ice emission signals simultaneously observed at microwave frequencies, in which ice permittivity is relatively well known. This empirical relationship also produces IWC values that agree well with the CALIOP, version 3.0, retrieval at values $<10\,\mathrm{mg\,m^{-3}}$. Because the microphysics assumption is critical in satellite cloud ice retrievals, the agreement found in the IWC–β_{532} relationships increase fidelity of the assumptions used by the lidar and microwave techniques for upper-tropospheric clouds.

1. Introduction

Cloud ice and occurrence frequency in the upper troposphere contribute significantly to Earth's total radiation and energy budgets. However, current climate and weather models produce a wide spread of values for these variables, leading to large uncertainties in the predicted dynamics and precipitation at the surface (e.g., Waliser et al. 2009; Eliasson et al. 2011; Jiang et al. 2012). Improving cloud ice retrieval and modeling is imperative and can be achieved by reducing uncertainty of the assumptions about cloud microphysics in remote sensing and modeling physics (e.g., Su et al. 2013).

Primary sources of the observed ice cloud microphysical properties are in situ measurements from high-altitude field campaigns, but these data are limited to the types of clouds and systems accessible by aircrafts. As a result, further assumptions and extrapolation are needed for global cloud systems, so that a generalized parameterization can be used to retrieve and model cloud ice and other properties (e.g., Zhao and Weng 2002; Heymsfield et al. 2005; Delanoë and Hogan 2008; Austin et al. 2009). Because of large uncertainties associated with the assumption/parameterization on cloud microphysics, satellite cloud ice retrievals remain different by a factor of 2 or more (e.g., Wu et al. 2009).

Corresponding author address: Dong L. Wu, M/S 33-C313, Climate and Radiation Laboratory (Code 613), NASA Goddard Space Flight Center, 8800 Greenbelt Road, Greenbelt, MD 20771. E-mail: dong.l.wu@nasa.gov

DOI: 10.1175/JAMC-D-13-041.1

© 2014 American Meteorological Society

Multiplatform multifrequency remote sensing now allows self-consistency evaluation of satellite cloud retrievals (e.g., cloud ice and cloud effective mass diameter D_{mm}). For example, passive microwave radiometers at 89 and 150 GHz (Zhao and Weng 2002), multifrequency radars (Majurec 2008; Matrosov 2011), and joint lidar–radar systems (Delanoë and Hogan 2008) were among the attempts of this sort. Unlike satellite versus ground-based observations, the cross validation among satellite sensors can be made on a global basis, but this requires coincident and collocated measurements and an overlapped sensitivity between sensors. The coincident measurements are generally uncommon among spaceborne platforms, but the National Aeronautics and Space Administration's (NASA) A-Train has collected an unprecedented amount of such measurements. NASA's A-Train is a set of satellites with multiple sensors that fly in formation on a sun-synchronous orbit (e.g., L'Ecuyer and Jiang 2010). The lidar–radar approach for cloud ice retrievals is applicable to the A-Train Cloud–Aerosol Lidar with Orthogonal Polarization (CALIOP) and *CloudSat* measurements, because the collocated footprints are within 1-min separation in time, or 400 km in distance along the track. However, there is a narrow overlap between lidar and radar in sensitivity and penetration, limiting the dynamic range of joint ice cloud retrievals using *CloudSat* and CALIOP. The overlapped clouds are often seen as a narrow layer in the A-Train curtain plots, at the bottom (top) of CALIOP (*CloudSat*) cloud profiles. Beyond the overlapped sensitivity range, cloud ice retrievals depend heavily on the individual sensor, for example, CALIOP for tenure cirrus and *CloudSat* for cumulonimbus.

In this study we evaluate the consistency of upper-tropospheric ice water content (IWC) measurements from another pair of A-Train sensors: CALIOP 532-nm backscatter and Microwave Limb Sounder (MLS) 240- and 640-GHz radiances. These remote sensing techniques are based on two independent ice cloud signals, namely light scattering (CALIOP) and ice emission (MLS) methods. For optically thin cirrus the MLS sensitivity comes from the blackbody emission of cloud ice over a long limb path, whereas CALIOP relies on the backscattering of cloud ice particles. In the case where ice particles are too small ($<10\,\mu$m) for *CloudSat* to detect cloud scattering signal (-30 dBZ), MLS can still detect the thermal emission of ice particles in the absence of scattering. The focus of our study is on the statistical consistency of satellite cloud ice measurements between a large ensemble of the datasets acquired at 15-km altitude after May 2008, when MLS and CALIOP samplings become nearly collocated and within 1 min apart along the A-Train curtain (Fig. 1).

2. Data and methods

Aura MLS, launched in July 2004, has seven radiometers with horizontal (H) and vertical (V) polarizations at frequencies near 118 (H, V), 190 (V), 240 (H), 640 (H) GHz and 2.5 (H, V) THz. MLS can detect ice clouds if the cloud top reaches MLS limb tangent heights h_t, but the sign of the cloud-induced radiance T_{cir}, the difference between the observed radiance and modeled clear-sky radiance after gas species retrievals are completed, is a function of h_t and cloud IWC or ice water path (IWP) in the limb line of sight (LOS; Wu et al. 2006, 2008, 2009). In the standard MLS cloud ice product, the 240-GHz T_{cir} is used for the IWC retrieval, while the T_{cir} at other frequencies are also computed and archived as diagnostic products. Comparing upper-tropospheric MLS 240-GHz and *CloudSat* IWC, Wu et al. (2009) found that MLS IWC retrieval is lower by as large as a factor of 5 at pressures <200 hPa. This large difference was thought to be mainly because of different assumptions about ice microphysics between these retrievals. The MLS retrieval uses the parameterization formulated by McFarquhar and Heymsfield (1997, hereafter MH97), whereas *CloudSat* assumes a gamma size distribution in cloud ice retrieval (Austin et al. 2009). Another factor that can cause the lower IWC is MLS sensitivity limitation. MLS cloud signals can become saturated in a very large IWC case. As a result, it reports the large IWC for a smaller value, causing a low bias in the MLS retrieval as IWC increases, which is evident in the MLS–*CloudSat* probability density function (PDF) comparison (Wu et al. 2009).

CALIOP is a dual-wavelength (532 and 1064 nm) and dual-polarization (perpendicular and parallel at 532 nm) lidar (Winker et al. 2009) that has footprints collocated with *CloudSat* 94-GHz cloud profiling radar (CPR; Stephens et al. 2002). The original level-1 β_{532} data have 583 vertical levels with resolutions from 30 m near the surface to 300 m in the stratosphere, and horizontal resolution of 300 m. CALIOP level-2 data [L2_05 kmCPro, version 3.0 (V3.0), dataset] contain extinction and IWC profiles at 60-m vertical and 5-km horizontal resolutions, which are retrieved from the β_{532} measurements. A detailed discussion of the CALIOP extinction coefficient retrieval can be found in Young and Vaughan (2009), where the inversion from the backscatter profile takes into account two-way molecular/particulate transmittance. For cloud extinction and IWC retrievals, the CALIOP version 3.01 (V3.01) algorithm assumes 25 ± 10 sr for the lidar ratio, 0.6 for multiple-scattering factor (Powell et al. 2010), and a temperature-invariant relation (IWC = $26\sigma^{1.22}$) for the extinction-to-IWC retrieval, where these coefficients correspond to the parameters at -73°C in (Heymsfield et al. 2005). Because the extinction

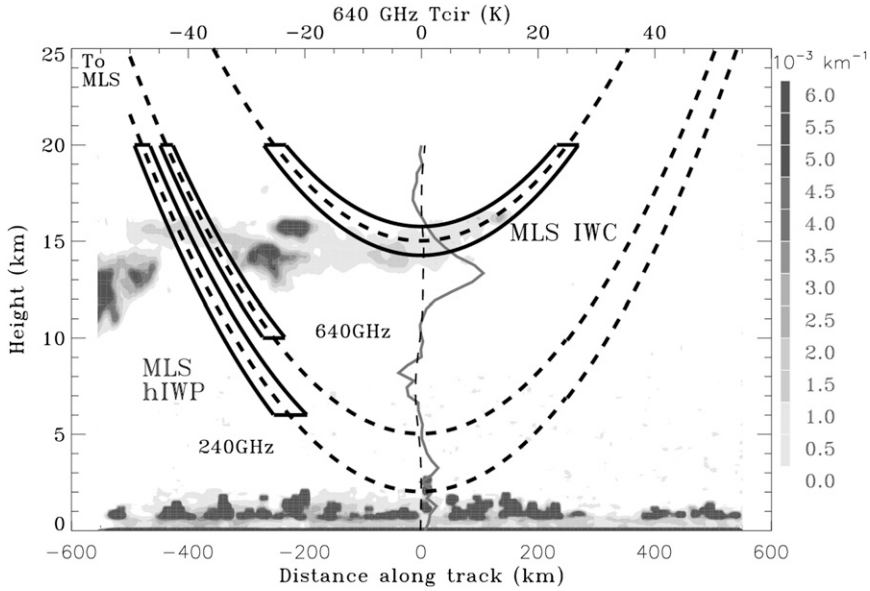

FIG. 1. A-Train MLS, CALIOP, and *CloudSat* cloud measurements on 19 May 2008 near 57.1°W, 13.5°N. The shaded contours are the attenuated CALIOP 532-nm backscatters. The MLS measurement volumes are indicated by the curved boxes. At high h_t MLS radiances can penetrate through the atmosphere limb to measure IWC. At low h_t, MLS radiances cannot see through the tangent point but can be used to measure IWP. The observed MLS 640-GHz ΔT_{cir} profile (the gray curve in the middle) shows a peak of approximately 10 K at $h_t \sim 14$ km, whereas the dashed profile is the calculated 640-GHz ΔT_{cir} from *CloudSat* IWC because the radar reports little IWC in this region because of the lack of sensitivity to small ice crystals.

and backscatter are linearly related, the CALIOP IWC is proportional to $\beta_{532}^{1.22}$. As shown in Fig. 2, for small ($<50 \times 10^{-3}\,\mathrm{km^{-1}\,sr^{-1}}$) β_{532} values, the retrieved IWC can be approximated by $0.29\beta_{532}^{1.22}$, where the linear slopes of 0.4 and $0.6\,\mathrm{g\,m^{-3}}$ $(\mathrm{km^{-1}\,sr^{-1}})^{-1}$ correspond to the gradient at 2 and $11\,\mathrm{mg\,m^{-3}}$, respectively.

Collocation between MLS and CALIOP measurements was not available during the early period of the CALIOP mission. A critical adjustment in the A-Train formation configuration was made in early 2008. Since then *Aura* MLS and CALIOP footprints are brought within ±10 km in the cross-track direction. The A-Train reconfiguration was completed in May 2008, and also improved the MLS-CALIOP temporal separation from ~7 to <1 min. This close alignment among A-Train sensors is critical for cloud studies, because large spatiotemporal variability may exist in upper-tropospheric clouds, especially those from deep convective systems.

In this study we use the version 2 240- and 640-GHz T_{cir} that were output as diagnostic products at the end of MLS retrieval process. The variable T_{cir} is defined as the difference between the observed and modeled radiances, where the modeled radiance is obtained from the radiative transfer calculation using the best estimated clear-sky atmospheric state (e.g., pressure P and temperature T) and gas profiles (e.g., H_2O and O_3). For CALIOP we use the version 3.0 532-nm attenuated total backscatter coefficient β_{532} and IWC data. To match the CALIOP and MLS measurement volumes, we integrate the CALIOP data along the MLS LOS (Fig. 1) to obtain a horizontally integrated IWC [i.e., horizontal ice water path (hIWP)] and integrated 532-nm backscatter γ_{532}, mathematically:

$$\mathrm{hIWP}(h_t) = \int_{-\infty}^{\infty} \mathrm{FOV}(z - h_t) \int_{\mathrm{LOS}} \mathrm{IWC}(s, z)\, ds\, dz \qquad (1)$$

and

$$\gamma_{532}(h_t) = \int_{-\infty}^{\infty} \mathrm{FOV}(z - h_t) \int_{\mathrm{LOS}} \beta_{532}(s, z)\, ds\, dz, \qquad (2)$$

where $\mathrm{FOV}(z)$ is the MLS field of view at tangent height z, approximately Gaussian, with a frequency-dependent beamwidth. In essence, γ_{532} is a proxy for visible optical depth along MLS LOS after scaled by the lidar ratio (i.e., extinction-to-backscatter ratio). The derived hIWP and γ_{532} are a function of MLS tangent height. At around 15-km tangent height, approximately speaking, hIWP is the IWC integrated over a distance of 200–300 km.

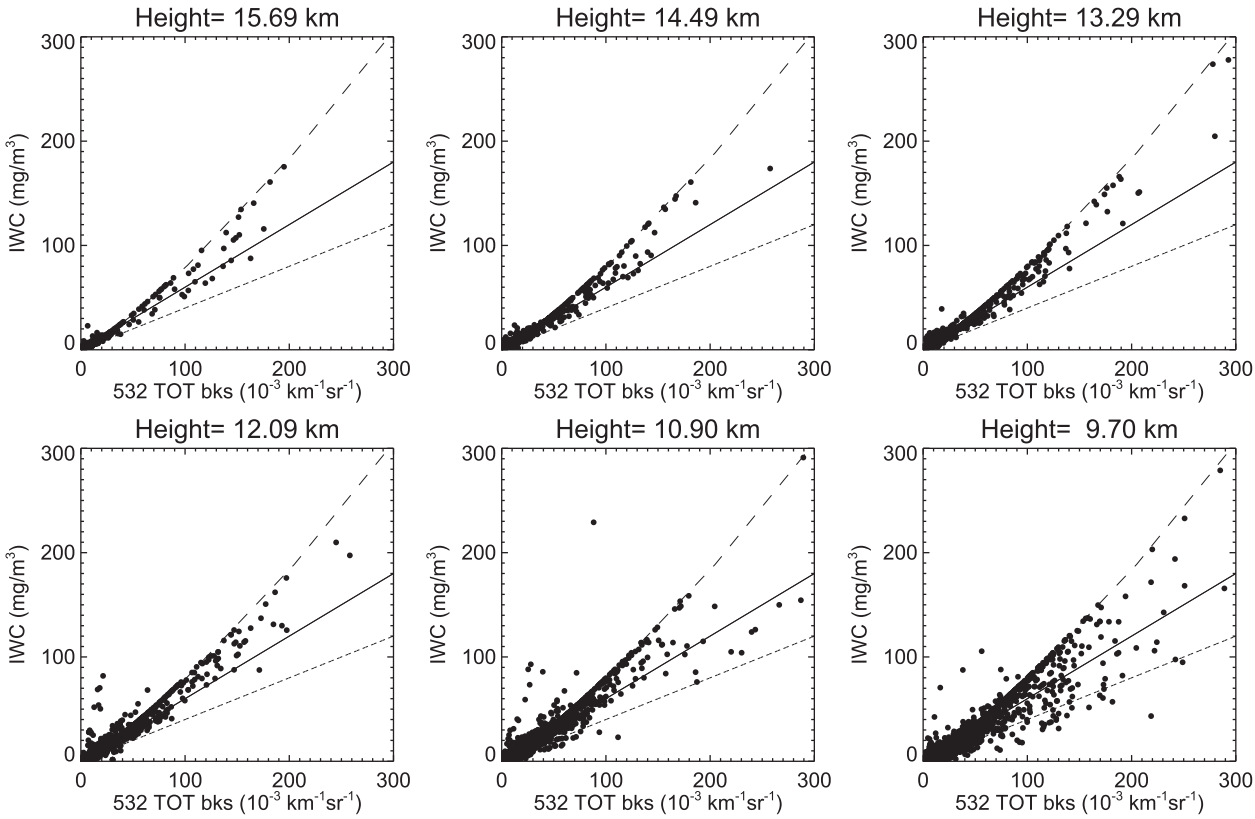

FIG. 2. The IWC–backscatter relationship from CALIOP V3.01 retrievals at selected height levels for 1 Jan 2007. The linear relationships with a slope of 0.4 and 0.6 g m^{-3} (km^{-1} sr^{-1})$^{-1}$, and the curve IWC = $0.29\beta_{532}^{1.22}$ are drawn for comparison (see text). The 532-nm backscatter coefficient from CALIOP V3.01 L2_05 kmCPro dataset is the original attenuated backscatter measurement.

The integrals in Eqs. (1) and (2) neglect the cloud self-extinction effect, which is valid as long as γ_{532} values are small (<1) along the MLS LOS. Variability of cloud inhomogeneity along the LOS may increase the noisy nature of comparisons between the matched datasets. However, deep convective cores occur at a much lower frequency than cirrus in the upper troposphere. In this study, we are interested in the cases where $\gamma_{532} < 1$ and these clouds are assumed to be mostly homogeneous. This volume-matching approach was also used by Wu et al. (2009) in comparing MLS and *CloudSat* cloud ice measurements.

3. CALIOP and MLS sensitivities to IWC

Three independent measurements, γ_{532}, T_{cir} (240 GHz), and T_{cir} (640 GHz), all sensitive to IWC, are used to evaluate consistency of the microphysics assumptions that lead to their cloud ice retrievals. Here we focus on the 15-km tangent height because CALIOP has relatively good sensitivity to cirrus without much saturation from thick cirrus. Most of the cloud IWC values at 15 km are small (<10 mg m^{-3}), and therefore it is reasonable to assume these variables (β_{532}, γ_{532}, T_{cir}, IWC, and hIWP) are linearly related to each other. Assuming for small cloud perturbations, these variables are basically the first term of the Taylor expansion of radiative transfer equation at a mean atmospheric state. Now, the question is whether these linear relations and underlying microphysics assumptions are consistent.

Without the CALIOP data, it is difficult to determine MLS T_{cir} sensitivity to IWC values because of large measurement error in MLS T_{cir}. As long as the T_{cir} error is random, we can extract its sensitivity to cloud ice from a large volume of MLS T_{cir} data by sorting them with respect to the collocated CALIOP γ_{532} measurements. As shown in the density distributions in Fig. 3, a weak linear correlation between T_{cir} and γ_{532} at $\gamma_{532} < 1$ emerges from the statistics of the collocated A-Train data, showing a statistically significant slope with the relative error better than 50% (as seen later in the fitted results). This relationship is expected for thermal emission of cloud ice at microwave frequencies, like those from atmospheric gases. Wu and Jiang (2004) and Wu et al. (2005) studied the sensitivity of MLS 203-GHz limb radiances to cloud ice in the upper troposphere, and

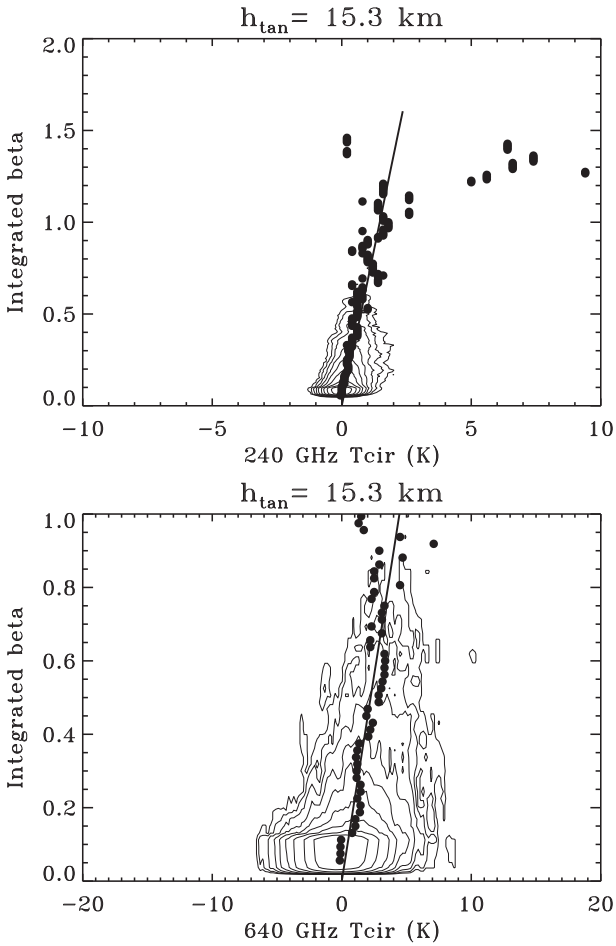

FIG. 3. Observed relations between CALIOP γ_{532} along MLS limb path and MLS 15-km $\Delta T_{\rm cir}$ at (top) 240 and (bottom) 640 GHz. A total of approximately 12 000 collocated CALIOP and MLS samples are used. The path integration of CALIOP backscatter along MLS LOS takes into account MLS field-of-view (FOV) effects. Contours are in a logarithmic scale, depicting the density distribution of the measurements. The black dots represent the most probable $\Delta T_{\rm cir}$ value at each γ_{532} bin. The line is a fit through these values, producing Eqs. (5) and (6). A bias in $\Delta T_{\rm cir}$ (-2.2 K for 240 GHz and -1.5 K for 640 GHz), because of modeled error in the clear-sky radiance, has been removed.

concluded that for small IWCs cloud ice emission can become a dominant process in the $T_{\rm cir}$–hIWP relationship in the tropopause region.

As IWC increases, so does the number of large-size ice particles. As a result, scattering becomes more important in the $T_{\rm cir}$–hIWP relationships. This transition is evident in Fig. 3, where the $T_{\rm cir}$–γ_{532} correlation switches drastically from the steep slope to a shallower slope at $\gamma_{532} > 1$ and $T_{\rm cir}$(240 GHz) > 2 K. The transition from emission to scattering-dominant $T_{\rm cir}$–γ_{532} relationship is frequency dependent because the scattering efficiency varies with frequency. In the MLS version 2.2 (V2.2) algorithm, only values with $T_{\rm cir}$ (240 GHz) $> \sim 1.5$ K (3σ) is considered as useful for cloud ice retrievals, whereas $T_{\rm cir}$ (240 GHz) < 1.5 K or $T_{\rm cir}$ (640 GHz) < 5 K are under the noise floor and classified as "clear sky." Thanks to CALIOP, now these cloud ice signals can be studied even within the MLS 240- and 640-GHz clear-sky radiances. The MLS measurements are generally consistent with the analysis in Eriksson et al. (2011), who studied the emission-scattering ratio for 348-GHz limb radiances at 14-km tangent height and found that the emission of cloud ice contributes ~20% to the total $T_{\rm cir}$ at large $T_{\rm cir}$ values. Their study also suggested an increased (~50%) contribution from ice emission as the 348-GHz limb $T_{\rm cir}$ decreases.

In the case where cloud ice is small (<10 mg m^{-3}), the $T_{\rm cir}$ dependence on IWC can be modeled relatively well from the measured ice dielectric properties at the microwave frequencies. There exists a simple linear $T_{\rm cir}$–IWC relationship in this case. As described in Wu and Jiang (2004), the radiative transfer calculation can be greatly simplified for small ($<10\,\mu$m) ice crystal and small (<10 mg m^{-3}) IWC value situations, under which cloud scattering is negligible. As a result, $T_{\rm cir}$ is directly proportional to IWC, similar to the radiance from clear-sky gas emissions. Furthermore, as shown below, we may have an analytical form to characterize the $T_{\rm cir}$–IWC relationship.

Consider the microwave radiances in form of $T_b = T_0[1 - e^{-(\tau_0 + \Delta\tau_{\rm cir})}]$, where T_0 is the ambient air temperature, τ_0 is the gaseous optical depth along MLS LOS, and $\Delta\tau_{\rm cir}$ is the cloud-induced optical depth. For $\Delta\tau_{\rm cir} \ll 1$, T_b may be approximately written as

$$T_b \approx T_0[1 - e^{-\tau_0}(1 - \Delta\tau_{\rm cir})] = T_0[1 - e^{-\tau_0}] + T_0 e^{-\tau_0},$$

where $T_{b0} \equiv T_0[1 - e^{-\tau_0}]$ is clear-sky background radiance, and $T_{\rm cir}$ is defined by

$$T_{\rm cir} \equiv T_b - T_{b0} \approx T_0 e^{-\tau_0} \Delta\tau_{\rm cir}.$$

If scattering is neglected, the cloud-induced optical depth becomes

$$\Delta\tau_{\rm cir} = 2.1 \frac{\rm IWC}{\lambda} \frac{3\varepsilon''}{(\varepsilon' + 2)^2 + \varepsilon''^2} \Delta s,$$

where hIWP = IWC $\cdot\, \Delta s$ as a simplified form of Eq. (1). Here, Δs is MLS pathlength in kilometers, IWC is in milligrams per cubic meter (mg m^{-3}, throughout this paper), wavelength λ is in centimeters, and (ε', $-\varepsilon''$) are real and imaginary part of ice dielectric constant (Jiang and Wu 2004). At approximately 15 km, within 5% of their variability, the typical values of T_{b0} in the tropics

are around 40 and around 135 K for MLS 240- and 640-GHz radiances, respectively, and $T_0 \sim 200$ K is used for the ambient clear-sky air temperature near the tropopause. With these approximate values, we have

$$T_{\mathrm{cir}}(240\,\mathrm{GHz}) \approx 2.4 \times \mathrm{IWC} \times \Delta s \tag{3}$$

and

$$T_{\mathrm{cir}}(640\,\mathrm{GHz}) \approx 7.8 \times \mathrm{IWC} \times \Delta s, \tag{4}$$

which yield a 240- to 640-GHz T_{cir} ratio of 1:3.3. Since the ice permittivity is known 10% accuracy at microwave frequencies (e.g., Jiang and Wu 2004), the coefficients in Eqs. (3) and (4) are relatively robust, compared to other error sources as discussed below.

The microwave cloud properties in Eqs. (3) and (4) are further used to verify or constrain CALIOP IWC retrieval in Fig. 2. From Fig. 3 we have

$$\frac{\gamma_{532}}{T_{\mathrm{cir}}} \approx 0.77\,(0.31) \quad \text{for} \quad 240\,\mathrm{GHz} \tag{5}$$

and

$$\frac{\gamma_{532}}{T_{\mathrm{cir}}} \approx 0.23\,(0.12) \quad \text{for} \quad 640\,\mathrm{GHz}. \tag{6}$$

The number in parentheses is the standard deviation of the fitted slope. Note that the 240- to 640-GHz T_{cir} ratio from Eqs. (5) and (6) is 1:3.4, close to the analytical value of 1:3.3 from the simple model in Eqs. (3) and (4). Substituting Eqs. (3) and (4) into Eqs. (5) and (6) and taking the fact that $\gamma_{532} = \beta_{532}\Delta s$, we have

$$\frac{\mathrm{IWC}}{\beta_{532}} \approx 0.61\,(0.20) \quad \text{for} \quad 240\,\mathrm{GHz} \tag{7}$$

and

$$\frac{\mathrm{IWC}}{\beta_{532}} \approx 0.57\,(0.14) \quad \text{for} \quad 640\,\mathrm{GHz}. \tag{8}$$

Both MLS channels suggest that the lidar IWC–β_{532} coefficient should be approximately 0.6 to satisfy the microwave cloud properties expected from purely ice thermal emission. By averaging the coefficients in Eqs. (7) and (8), we obtain an empirical coefficients for the IWC–β_{532} relationship,

$$\mathrm{IWC} = (0.58 \pm 0.11)\beta_{532}, \tag{9}$$

where β_{532} is in inverse kilometers per steradian. As shown in Fig. 2, the slope of 0.58 from Eq. (9) agrees quite well with the majority of CALIOP V3.0 retrievals at IWC $< 100\,\mathrm{mg\,m^{-3}}$. The agreement increases fidelity of the microphysics assumptions used by the CALIOP scattering and MLS emission techniques for cloud ice retrievals at approximately 15 km.

4. Discussion

The linear IWC–β_{532} relationship [Eq. (9)] derived in this study provides an independent evaluation on the CALIOP cloud ice retrieval in the V3.01 L2_05 kmCPro dataset. The key microphysics constraint in Eq. (9), however, is not scattering properties of ice crystals. Rather, it is based on the ice permittivity properties at 240 and 640 GHz, which determine the thermal emission of cloud ice and the T_{cir} sensitivity to IWC at these frequencies. In the case where IWC and ice particle sizes are small, scattering can be neglected at the MLS frequencies, which leads to the linear proportionality of T_{cir} to IWC. Since ice permittivity is well known at microwave frequencies (with 10% uncertainty; e.g., Jiang and Wu 2004), the uncertainty of Eq. (9) is dominated by the errors in the observed T_{cir}–γ_{532} relationships in Eqs. (5) and (6).

The agreement between IWC = $0.58\beta_{532}$ and CALIOP V3.0 retrieval appears to hold well for most altitudes. The increased scatters at lower altitudes in the CALIOP V3.0 data are likely induced by the noise in the extinction retrieval that is expected to increase at lower altitudes in the presence of more high clouds. There is a subtle difference in the IWC–β_{532} relation between Eq. (9) and CALIOP V3.0 at IWC $< \sim 2\,\mathrm{mg\,m^{-3}}$, showing a slope of 0.4, or approximately 50% smaller than 0.58, which would yield a low bias in the CALIOP V3.0 IWC retrieval compared to Eq. (9). At IWC $> 11\,\mathrm{mg\,m^{-3}}$, the slope in CALIOP V3.0 is greater than 0.6, which would produce a larger IWC retrieval than Eq. (9). The CALIOP V3.0 IWC retrieval employs several assumptions (e.g., lidar ratio, multiple-scattering factor, and extinction-to-IWC coefficient), among which the IWC–β_{532} relation was derived from the data with large scatters (Heymsfield et al. 2005). The agreement between CALIOP V3.0 and Eq. (9) suggests that the uncertainty associated with the CALIOP IWC retrieval should be <50%.

To further validate the CALIOP V3.0 and Eq. (9) IWC retrievals, we compare them with *CloudSat* data and statistics of in situ measurements in terms of normalized probability density function (PDF). As described in Wu et al. (2009), the normalized PDF is able to characterize measurement noise, bias, and sensitivity range (sensor noise and saturation), without requiring collocation as long as they have the same ensemble sampling.

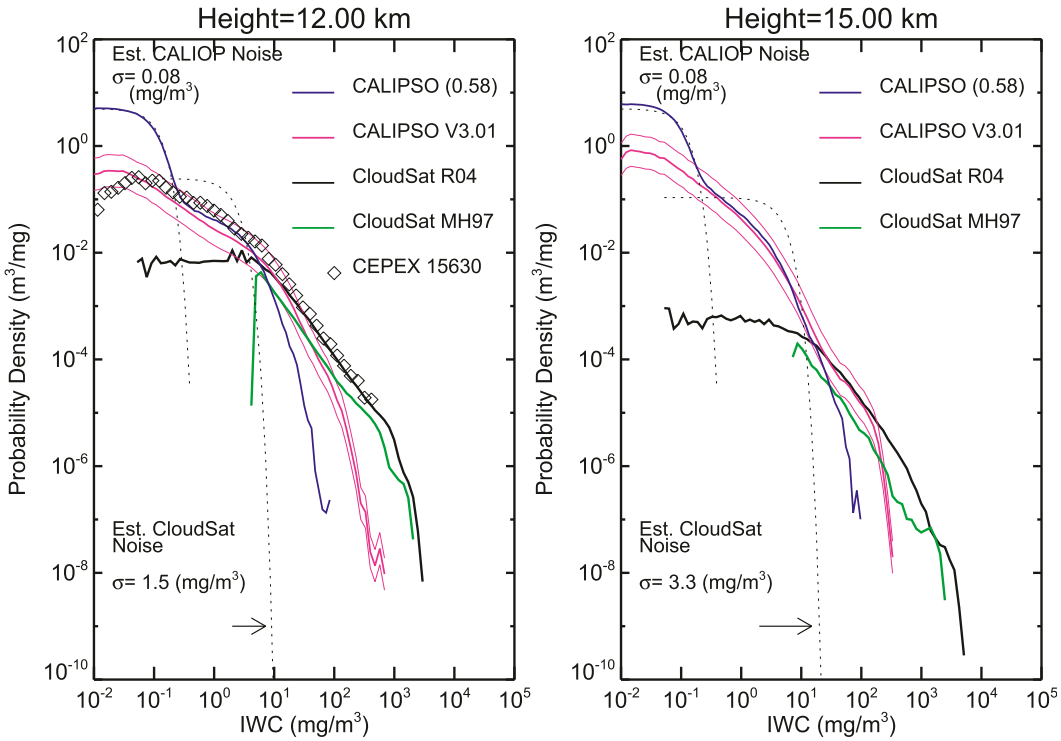

FIG. 4. Normalized PDFs of CEPEX, CALIOP, and *CloudSat* IWC at (left) 12 and (right) 15 km for July 2006 in a tropical band 2.5°S–2.5°N. *CloudSat* IWC retrievals from R04 (Austin et al. 2009) and from the MH97 size distribution are included for comparisons. The CALIOP V3.0 IWC PDF is bound by a scaling factor of 2 to guide comparisons. The CALIOP IWC measurement noise is estimated from the attenuated backscatter assuming the IWC = $0.58\beta_{532}$ relation, and the normalized Gaussian noise distribution is the dotted line. Similarly, the *CloudSat* IWC noise is estimated from the reflectivity measurements Z_e using the calculated Z_e–IWC relation. The estimated CALIOP and *CloudSat* IWC precisions are 0.08 at 1.5 mg m^{-3} at 12 km, and 0.08 and 3.3 mg m^{-3} at 15 km, using the method in Hogan et al. (2006). The PDF from the MH97 retrieval is cut off at 3σ to remove the portion below the *CloudSat* reflectivity noise (-27 dBZ).

Here we focus on the CALIOP IWC statistics for latitudes of 2.5°S–2.5°N in July 2006, with comparisons against in situ measurements obtained during Central Equatorial Pacific Experiment (CEPEX) at 12 km, and with *CloudSat* at 12 and 15 km. Two *CloudSat* IWC retrievals are included: one from the standard IWC product in the R04 release (Austin et al. 2009) and the other from the retrieval assuming the MH97 size distribution (Eriksson et al. 2008; Rydberg et al. 2009).

As seen in Fig. 4, there is good agreement between CALIOP and *CloudSat* R04 IWC PDFs at 12 and 15 km in the overlapped sensitivity ranges. The two sensors overlap for IWC values of 5–20 mg m^{-3} at 12 km and 30–200 mg m^{-3} at 15 km, respectively. The overlapped sensitivity requires the sensitivity from both instruments must be greater than their measurement noise but not saturated. Figure 4 shows that CALIOP PDFs drop off sharply at large IWC values, as expected for the increased attenuation by the dense cloud at a higher altitude. The attenuation correction, as implemented in the CALIOP V3.0 algorithm, can mitigate the problem to the extent where clouds are moderately thick. Thus, we should focus more on the comparison at small IWC values, where clouds are relatively thin and above the *CloudSat* detector noise (-31 dBZ), The *CloudSat* cloud ice PDF agrees with CALIOP V3.0 at 5–20 mg m^{-3} for 12 km and at 30–200 mg m^{-3} for 15 km. The reduced CALIOP sensitivity overlap with *CloudSat* at 12 km is, on one hand, a manifestation of increased attenuation from the clouds above. On the other hand, it is limited by the lower limit in *CloudSat* cloud detection. The *CloudSat* IWC noise produces a white PDF below its detection limit, corresponding to approximately 5 mg m^{-3} at 12 km and approximately 30 mg m^{-3} at 15 km, respectively.

Despite the reduced sensitivity overlap with *CloudSat* at 12 km, it is encouraging to observe the agreement between *CloudSat* and CALIOP cloud ice probability at the 5–20 mg m^{-3} range. More importantly, cloud ice statistics are extended for most cirrus with IWC between approximately 5 mg m^{-3} (3σ *CloudSat* noise) and

approximately 0.2 mg m^{-3} (3σ CALIOP noise). The CALIOP V3.0 PDF shows a slightly low bias against CEPEX PDF at IWC values between 0.5 and 5 mg m^{-3}. A plausible cause could be the cloudy-sky bias from the sampling during the CEPEX campaign. Another possibility, as aforementioned, is because of a smaller slope in the IWC–β_{532} conversion at IWC $< \sim 2$ mg m^{-3}, which would lower the probability at IWC near this value. On the other hand, the retrieval using Eq. (9) would produce a probability closer to the CEPEX statistics.

The 12 km is a critical altitude for *CloudSat* IWC validation against in situ measurements. As pointed out in Wu et al. (2009), the *CloudSat* R04 IWC statistics agree well with the CEPEX statistics over a broad range of IWC (5–1000 mg m^{-3}). In a comparison of MLS V2 and *CloudSat* R04 IWC, Wu et al. (2009) found that MLS mean IWC is lower by a factor of approximately 5 against *CloudSat* at 147 and 100 hPa. The microphysics assumption was thought to be the key cause of this difference. To further evaluate the impacts of the microphysics assumption on *CloudSat* IWC retrievals, we compare the IWC retrievals using the MH97 parameterization, as used in the MLS retrieval, to the R04 product (assuming a gamma size distribution). As shown in Fig. 4, the MH97 IWC retrieval lowers the PDF by a factor of approximately 2 and approximately 4 at 12 and 15 km, respectively. This is generally consistent with the study by Eriksson et al. (2008), showing that the mean IWC is lower by 1.3 at 12.5 km and 2.4 at 15.5 km. All these cross-satellite evaluations support the speculation that the lower bias in MLS IWC, which increases with height, was because of the MH97 size distribution assumption (Wu et al. 2009). On the other hand, the agreement of cloud ice measurements among *CloudSat*, CALIOP V3.0, and Eq. (9) at 15 km suggests that the gamma size distribution, as used by *CloudSat*, appears to be more realistic for upper-tropospheric ice clouds.

5. Conclusions

Analyzing a large ensemble of collocated A-Train CALIOP backscatter β_{532} and MLS cloud-induced radiance T_{cir} measurements, we obtained the empirical relationships among β_{532} and MLS 240- and 640-GHz T_{cir}. These linear relations are statistically significant and lead to an empirical extinction-to-IWC conversion in Eq. (9) for small IWC values, that is, IWC/β_{532} = 0.58 ± 0.11. The key microphysics assumption in Eq. (9) is the ice permittivity property at microwave frequencies, which is known to a good accuracy. Because of the noisy MLS measurements in small T_{cir} values, the uncertainty in Eq. (9) is dominated by the observed T_{cir}–γ_{532} relationships. Since MLS T_{cir}, is directly proportional to IWC and independent of the shape of particle size distribution for small IWC values, the resulting IWC–β_{532} relation provides additional constraint on the CALIOP cloud ice retrieval.

The empirical IWC–β_{532} relation in Eq. (9) agrees well with the extinction-to-IWC conversion used in the CALIOP V3.0 retrieval. This agreement improves fidelity of the scattering-based CALIOP and emission-based MLS IWC retrievals, as a result of the consistent microphysics in explaining the observed T_{cir}–γ_{532} correlation. Furthermore, the agreement between CALIOP and *CloudSat* IWC PDFs suggests that the MH97 parameterization be the primary cause of the underestimation of MLS cloud ice at 15 km and the altitudes above.

Finally, we demonstrate in this study that multisensor analyses can be used to constrain the microphysics assumptions used in satellite cloud ice retrievals. Through self-consistency evaluation on the collocated A-Train measurements, we are able to cross evaluate the cloud ice measurements at two extreme wavelengths: millimeter- and submillimeter-wave versus visible. Both emission-based microwave radiometry and scattering-based lidar backscattering reach a statistically consistent (<50%) IWC–β_{532} relationship on different assumptions about ice cloud microphysics in the upper troposphere. This agreement raises fidelity on these assumptions and sheds a new light on the issues unsolved by earlier cloud validation efforts. Similar studies can be applied to other A-Train sensor pairs or closely sampled datasets from formation flights.

Acknowledgments. Supports from NASA's *Aura*, *CloudSat*, and Earth System Data Records Uncertainty Analysis (ESDRERR) projects, as well as the data processing by the Langley Research Center Atmospheric Sciences Data Center and by *CloudSat* Data Processing Center, are gratefully acknowledged. The work at the Jet Propulsion Laboratory, California Institute of Technology, was performed under contract with NASA.

REFERENCES

Austin, R. T., A. J. Heymsfield, and G. L. Stephens, 2009: Retrievals of ice cloud microphysical parameters using the *CloudSat* millimeter-wave radar and temperature. *J. Geophys. Res.,* **114,** D00A23, doi:10.1029/2008JD010049.

Delanoë, J., and R. J. Hogan, 2008: A variational scheme for retrieving ice cloud properties from combined radar, lidar, and infrared radiometer. *J. Geophys. Res.,* **113,** D07204, doi:10.1029/2007JD009000.

Eliasson, S., S. A. Buehler, M. Milz, P. Eriksson, and V. O. John, 2011: Assessing observed and modelled spatial distributions

of ice water path using satellite data. *Atmos. Chem. Phys.,* **11,** 375–391, doi:10.5194/acp-11-375-2011.

Eriksson, P., M. Ekström, B. Rydberg, D. L. Wu, R. T. Austin, and D. P. Murtagh, 2008: Comparison between early Odin-SMR, *Aura* MLS and *CloudSat* retrievals of cloud ice mass in the upper tropical troposphere. *Atmos. Chem. Phys.,* **8,** 1937–1948.

——, B. Rydberg, and S. A. Buehler, 2011: On cloud ice induced absorption and polarization effects in microwave limb sounding. *Atmos. Meas. Tech.,* **4,** 1305–1318.

Heymsfield, A. J., D. Winker, and G.-J. van Zadelhoff, 2005: Extinction-ice water content-effective radius algorithms for *CALIPSO*. *Geophys. Res. Lett.,* **32,** L10807, doi:10.1029/2005GL022742.

Hogan, R. J., M. P. Mittermaier, and A. J. Illingworth, 2006: The retrieval of ice water content from radar reflectivity factor and temperature and its use in evaluating a mesoscale model. *J. Appl. Meteor.,* **45,** 301–317.

Jiang, J. H., and D. L. Wu, 2004: Ice and water permittivities for millimeter and sub-millimeter remote sensing applications. *Atmos. Sci. Lett.,* **5** (7), 146–151.

——, and Coauthors, 2012: Evaluation of cloud and water vapor simulations in CMIP5 climate models using NASA ''A-Train'' satellite observations. *J. Geophys. Res.,* **117,** D1410, doi:10.1029/2011JD017237.

L'Ecuyer, T. S., and J. H. Jiang, 2010: Touring the atmosphere aboard the A-Train. *Phys. Today,* **63** (7), 36–41, doi:10.1063/1.3463626.

Majurec, N., 2008: Advanced multi-frequency radar: Design, preliminary measurements and particle size distribution retrieval. Ph.D. dissertation, University of Massachusetts Amherst, Paper AAI3315523, 230 pp. [Available online at http://seasatmac.ecs.umass.edu/~siqueira/AMFR/catalog/00README/Majurec_Dissertation.pdf.]

Matrosov, S. Y., 2011: Feasibility of using radar differential Doppler velocity and dual-frequency ratio for sizing particles in thick ice clouds. *J. Geophys. Res.,* **116,** D17202, doi:10.1029/2011JD015857.

McFarquhar, G. M., and A. J. Heymsfield, 1997: Parameterization of tropical cirrus ice crystal size distributions and implications for radiative transfer: Results from CEPEX. *J. Atmos. Sci.,* **54,** 2187–2200.

Powell, K., and Coauthors, 2010: *CALIPSO* quality statements: Lidar level 2 cloud and aerosol layer products (version release: 3.01). NASA Atmospheric Science Data Center, 27 pp. [Available online at https://eosweb.larc.nasa.gov/sites/default/files/project/calipso/quality_summaries/CALIOP_L2LayerProducts_3.01.pdf.]

Rydberg, B., P. Eriksson, S. A. Buehler, and D. P. Murtagh, 2009: Non-Gaussian Bayesian retrieval of tropical upper tropospheric cloud ice and water vapour from Odin-SMR measurements. *Atmos. Meas. Tech.,* **2,** 621–637.

Stephens, G. L., and Coauthors, 2002: The *CloudSat* mission and the A-Train. *Bull. Amer. Meteor. Soc.,* **83,** 1771–1790.

Su, H., and Coauthors, 2013: Diagnosis of regime-dependent cloud simulation errors in CMIP5 models using A-Train satellite observations. *J. Geophys. Res. Atmos.,* **118,** 2762–2780, doi:10.1029/2012JD018575.

Waliser, D. E., and Coauthors, 2009: Cloud ice: A climate model challenge with signs and expectations of progress. *J. Geophys. Res.,* **114,** D00A21, doi:10.1029/2008JD010015.

Winker, D. M., and Coauthors, 2009: Overview of the *CALIPSO* mission and CALIOP data processing algorithms. *J. Atmos. Oceanic Technol.,* **26,** 2310–2323.

Wu, D. L., and J. H. Jiang, 2004: EOS MLS algorithm theoretical basis for cloud measurements. JPL D-19299, 128 pp. [Available online at http://mls.jpl.nasa.gov/data/eos_cloud_atbd.pdf.]

——, W. G. Read, A. E. Dessler, S. C. Sherwood, and J. H. Jiang, 2005: UARS MLS cloud ice measurements and implications for H_2O transport near the tropopause. *J. Atmos. Sci.,* **62,** 518–530.

——, J. H. Jiang, and C. Davis, 2006: EOS MLS cloud ice measurements and cloudy-sky radiative transfer model. *IEEE Trans. Geosci. Remote Sens.,* **44,** 1156–1165.

——, and Coauthors, 2008: Validation of the *Aura* MLS cloud ice water content measurements. *J. Geophys. Res.,* **113,** D15S10, doi:10.1029/2007JD008931.

——, and Coauthors, 2009: Comparisons of global cloud ice from MLS, *CloudSat,* and correlative data sets. *J. Geophys. Res.,* **114,** D00A24, doi:10.1029/2008JD009946.

Young, S. A., and M. A. Vaughan, 2009: The retrieval of profiles of particulate extinction from *Cloud-Aerosol Lidar Infrared Pathfinder Satellite Observations* (*CALIPSO*) data: Algorithm description. *J. Atmos. Oceanic Technol.,* **26,** 1105–1119.

Zhao, L., and F. Weng, 2002: Retrieval of ice cloud parameters using the Advanced Microwave Sounding Unit. *J. Appl. Meteor.,* **41,** 384–395.